Ms. for Dalton Trans. (paper ref.: DT-ART-01-2017-000378, revised)

Octahedral manganese(I) and ruthenium(II) complexes containing 2-(methylamido)pyridine–borane as a tripod κ^3*N,H,H*-ligand†

Javier Brugos,[a] Javier A. Cabeza*[a] Pablo García-Álvarez,[a] Enrique Pérez-Carreño[b] and Juan F. Van der Maelen[b]

[a]*Centro de Innovación en Química Avanzada (ORFEO-CINQA), Departamento de Química Orgánica e Inorgánica-IUQOEM, Universidad de Oviedo-CSIC, 33071 Oviedo, Spain*

[b]*Departamento de Química Física y Analítica, Universidad de Oviedo, 33071 Oviedo, Spain*

† Electronic supplementary information (ESI) available: NMR spectra and XRD and QTAIM data. CCDC 1524082 (**1**) and 1524083 (**2**). For ESI and crystallographic data in CIF or other electronic format see DOI: 10.1039/00000000.

Abstract: The borane adduct of the 2-(methylamido)pyridine anion, $[mapyBH_3]^-$, has been incorporated to octahedral metal complexes. In *fac*-[Mn(κ^3*N,H,H*-mapyBH$_3$)(CO)$_3$] (**1**) and *fac*-[RuH(κ^3*N,H,H*-mapyBH$_3$)(CO)(P*i*Pr$_3$)] (**2**), which have been prepared by treating K[mapyBH$_3$] with *fac*-[MnBr(MeCN)$_2$(CO)$_3$] and [RuHCl(CO)(P*i*Pr$_3$)$_2$], respectively, it behaves as a tripod ligand, attached to the metal atom through the amido N atom and through two H atoms of the BH_3 moiety. X-ray diffraction analyses and theoretical studies (DFT, QTAIM) have shown that the MH_2B atom grouping of **1** and **2** comprises two 3c–2e M–H–B interactions that are between those of Shimoi type (κ^1*H* coordination of the B–H bond) and those of agostic type (κ^2*B*,*H* coordination of the B–H bond). However, while both M–H–B interactions are almost identical in complex **1**, this is not the case in complex **2**, in which one M–H–B interaction is more agostic than the other due to the different *trans* influence of the hydride and phosphane ligands.

Introduction

The coordination chemistry of amine–boranes[1–4] (H_2RNBH_2R'; R, R' = H, alkyl, aryl) and aminoboranes[4,5] (HRNBHR'; products that arise from the dehydrogenation of amine–boranes) is currently a very active research field because some transition-metal complexes have been found to promote the catalytic dehydrogenation of amine–boranes[1–3] (release of H_2) and/or the transfer of some of their H atoms to other molecules (transfer hydrogenation reactions).[6] In their transition-metal complexes, amine–boranes and aminoboranes use one or two of their BH groups to bind the metal atom (σ-complexes), implicating only the H atom (Shimoi-type coordination) or both B and H atoms (agostic-type coordination) of the B–H bond.[7]

The coordination chemistry of some borane adducts of potentially bidentate Lewis bases has recently started to be studied. In the complexes known so far, these ligands use one[8–13] or two[8c,11,12j,13,14] borane H atoms and an additional donor atom (E) to bind the metal atom (κ^2*E*,*H* and κ^3*E*,*H*,*H*, respectively). Currently, the only transition metal complexes that are known to contain borane adducts as κ^3*E*,*H*,*H*-ligands are those represented in Fig. 1, which are derived from diphosphanes,[11] benzothiazolate,[8c] phosphoramidate,[13] and 2-(methylamido)pyridine.[14] A hemilabile behavior of these tridentate ligands (the BH–M interactions are weak) has been observed in a few occasions.[11b,11c]

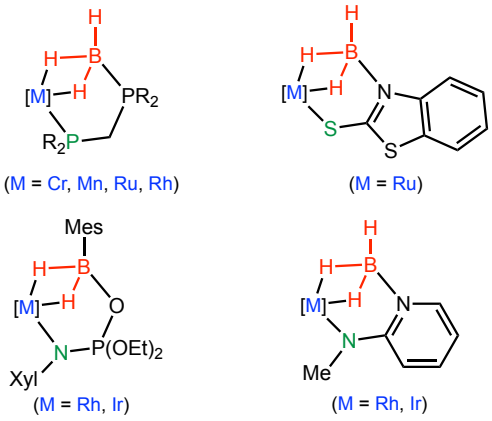

Fig. 1 Transition metal complexes containing a borane–Lewis base ligand coordinated through two borane H atoms and through an additional donor group (references are given in the text).

In this context, we have described the synthesis of the pentacoordinated complexes [M(κ^3*N,H,H*-mapyBH_3)(cod)] (M = Rh, Ir; Hmapy = 2-(methylamino)pyridine; cod = cycloocta-1,5-diene; Fig. 1),[14] which are the first metal complexes derived from 2-(methylamino)pyridine–borane (HmapyBH_3). In solution at room temperature, the BH_3 group of these complexes rotates about the B–N bond averaging the three B–H

bonds. X-ray diffraction (XRD) and Density Functional Theory (DFT) and Quantum Theory of Atoms in Molecules (QTAIM) calculations demonstrated that in solid state and in gas phase they are trigonal bipyramidal complexes having two equatorial coordination sites occupied by M–HB interactions that, interestingly, are between those of Shimoi-type (κ^1*H* coordination of the B–H bond) and those of agostic-type (κ^2*B*,*H* coordination of the B–H bond) but one is more agostic than the other, resulting in an asymmetric MH_2B atom grouping. Such an asymmetric coordination of the H_2B group was associated with its narrow H–M–H bite angle (62° in the Rh complex and 70° in the Ir one), since a symmetric coordination of the H_2B fragment to two equatorial sites of a trigonal bipyramidal metal complex (the ideal coordination angle is 120°) would imply either too short M–HB distances or too small overlaps between the metal orbitals and the orbitals of the H_2B group. The off-center location of the ring critical point (QTAIM study) associated with the MH_2B atom grouping provided a straightforward visual indication of the asymmetric coordination of the BH_2 group in these complexes.[14] An asymmetric coordination of an H_2B group was never identified before, although it may have been overlooked (at least in trigonal bipyramidal complexes) because the accuracy in determining the position of H atoms attached to transition metal atoms by XRD is generally low and also because the synthesis and characterization of the currently known complexes of this type have not been accompanied with appropriate theoretical studies.

The above precedents prompted us to check whether or not the coordination of the H_2B group of a κ^3*N,H,H*-mapyBH_3 ligand is also asymmetric in octahedral complexes, in which the ideal coordination angle, 90°, is 30° narrower than the trigonal bipyramidal equatorial angle. We now report the synthesis and structural characterization of the octahedral complexes *fac*-[Mn(κ^3*N,H,H*-mapyBH_3)$(CO)_3$] (**1**) and *fac*-[RuH(κ^3*N,H,H*-mapyBH_3)(CO)(P*i*Pr_3)] (**2**) and DFT and QTAIM theoretical studies focused on the interactions between the atoms of the MH_2B part of these complexes. We chose these two complexes because the symmetry of their MH_2B atom grouping was not expected to be influenced by the *a priori* symmetric arrangement of the ligands in complex **1**, but, on the contrary, it might be affected by the inevitable asymmetric arrangement of the ligands in complex **2**.

Results and discussion

Compounds **1** and **2** were synthesized by treating [Mn$Br(MeCN)_2(CO)_3$] or [RuHCl(CO)(P*i*$Pr_3)_2$], respectively, with a toluene solution of K[mapyBH_3] (prepared *in situ* by deprotonating HmapyBH_3 with K[N$(SiMe_3)_2$]) at room temperature (Scheme 1). They were isolated as orange (**1**) and yellow (**2**) solids in good yields (> 60%).

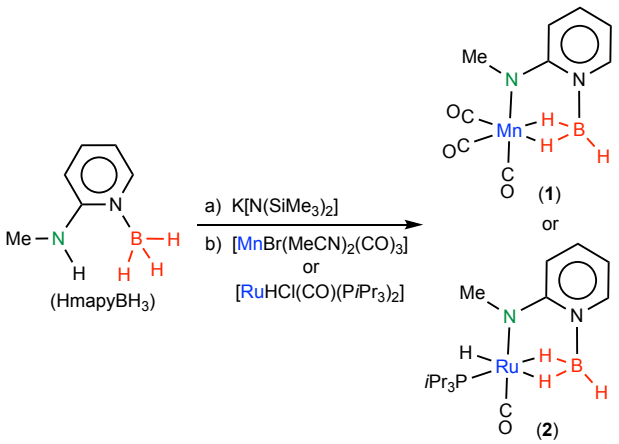

Scheme 1 Synthesis of compounds **1** and **2**.

The facial arrangement of the carbonyl ligands of complex **1** was suggested by its IR spectrum in toluene, which showed two ν_{CO} absorptions at 2040 (s) and 1951 (vs, br) cm^{-1}. Its NMR spectra confirmed a C_S molecular symmetry, since its carbonyl ligands led to two resonances in the $^{13}C\{^1H\}$ spectrum, δ_{13C} 222.4 and 219.1 in C_6D_6, with a 2:1 intensity ratio, and the BH_3 group also led to two resonances in the ^1H spectrum, δ_{1H} 4.31 (1 H) and –10.17 (2 H), which were observed as very broad quartets due to coupling to ^{11}B (I = 3/2), $J_{1H\text{-}11B}$ = 129 and 71 Hz, respectively, but as singlets in a $^1H\{^{11}B\}$ spectrum (slightly broadened by the ^{55}Mn nucleus, I = 5/2). Consequently, the ^{11}B NMR spectrum of **1** contained a doublet of triplets with $J_{1H\text{-}11B}$ coupling constants comparable with those observed in the ^1H NMR spectrum (images of all these spectra are contained in the Electronic Supplementary Information (ESI), Fig. S1 and S2). All these NMR data, which were obtained in C_6D_6 solution at 298 K, indicate that compound **1** is rigid under these conditions. However, at room temperature and above, the BH_3 group of the previously reported complexes [M(κ^3*N,H,H*-mapyBH$_3$)(cod)] (M = Rh, Ir) was found to be involved in a fluxional process that interchanges the three H atoms (rotation of the BH_3 group about the B–N bond).[14]

The analytical and spectroscopic data of the ruthenium complex **2** confirmed its composition and the presence of one hydride, one phosphane, one CO, and one mapyBH$_3$ ligand, but they did not help to unambiguously assign the ligand positions, which were subsequently determined by XRD (see below). In addition to the signals of the phosphane and mapy groups, the ^1H NMR spectrum of **2** (ESI, Fig. S3) contained three very broad quartets, δ_{1H} 4.45 ($J_{1H\text{-}11B}$ = 113 Hz), –4.35 ($J_{1H\text{-}11B}$ = 65 Hz) and –6.52 ($J_{1H\text{-}11B}$ = 65 Hz), and a sharp doublet, δ_{1H} –11.68 ($J_{H\text{-}P}$ = 24.0 Hz). While the last signal clearly belongs to the hydride ligand, the three broad quartets belong to the protons of

the BH_3 group, since they were transformed into a triplet (J_{1H-1H} = 8.0 Hz), a broad singlet and a doublet (J_{1H-31P} = 8.0 Hz), respectively, in a $^1H\{^{11}B\}$ NMR spectrum. The J_{1H-11B} coupling constants observed in the ^1H NMR spectrum were also measured in the doublet of triplets observed in a ^{11}B NMR spectrum (ESI, Fig. S4). These NMR data, which were obtained in C_6D_6 solution at 298 K, indicate that, as complex **1**, complex **2** is stereochemically rigid in solution at room temperature.

The molecular structures of complexes **1** and **2**, obtained from XRD analyses performed at 145(2) K (**1**) and 151(2) K (**2**), are shown in Fig. 2 and 3, respectively. In addition to confirming the tripod κ^3*N,H,H* coordination of the mapyBH_3 ligand in both cases, they also indicate the coordination positions of the remaining ligands, including those of the carbonyl, hydride and phosphane ligands of complex **2**, whose locations could not be unambiguously inferred from spectroscopic data.

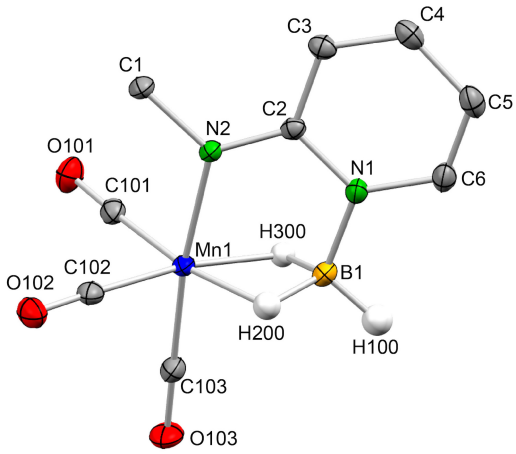

Fig. 2 XRD molecular structure of compound **1** (thermal ellipsoids set at 30 % probability). Selected interatomic distances and angles are given in Table 1.

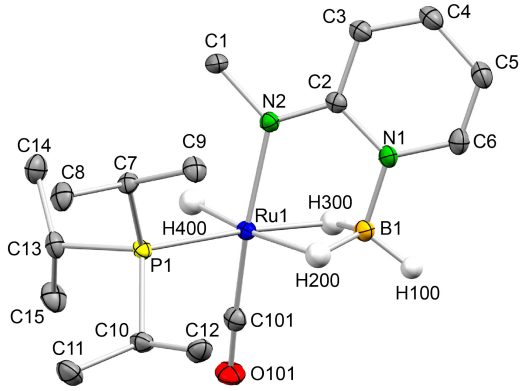

Fig. 3 XRD molecular structure of compound **2** (thermal ellipsoids set at 30 % probability). Selected interatomic distances and angles are given in Table 2.

A careful inspection of the metrics concerning the Mn atom and the atoms of the BH_3 group of complex **1** revealed that those involving H200 (Mn1−H200 1.66(2) Å,

B1−H200 1.21(2) Å, Mn1–H200–B1 95.2(13)^{o}) are slightly different from those involving H300 (Mn1−H300 1.71(2) Å, B1−H300 1.24(2) Å, Mn1–H300–B1 91.9(12)^{o}) and that the B1–H100 distance (1.09(2) Å) is *ca.* 0.2 Å shorter than the other B–H distances. The Mn1···B1 distance is 2.144(2) Å. Regarding complex **2**, the metrics involving H200 (Ru1−H200 1.83(3) Å, B1−H200 1.28(3) Å, Ru1–H200–B1 89.2(15)^{o}) are almost identical to those involving H300 (Ru1−H300 1.80(3) Å, B1−H300 1.28(3) Å, Ru1–H300–B1 90.4(15)^{o}), despite the *trans* influence of hydride ligands is known to be stronger than that of phosphane ligands.[15] The Ru1···B1 distance is 2.213(2) Å.

As the XRD metrics involving the H200 and H300 atoms of **1** and **2** might be affected by experimental errors (some differences are within the estimated standard deviations) and also by packing effects in the solid state, we decided to optimize by DFT methods the gas phase molecular structures of **1** and **2** without symmetry restraints. The results obtained from relativistic (ZORA-PW91) and non-relativistic (B3P86) approaches are compared with the experimental ones (XRD) in Tables 1 and 2. Interestingly, both theoretical methods rendered very similar symmetric C_S structures for complex **1** (Table 1), while they maintained a small asymmetry in the metrics associated with the RuH_2B part of complex **2** (Table 2).

Table 1. Experimental (XRD) and calculated (DFT) interatomic distances (Å) and angles (^{o}) in *fac*-[Mn(κ^3*N,H,H*-mapyBH_3)$(CO)_3$] (**1**)

Atoms	XRD	ZORA-PW91/QZ4P	B3P86/6-31G(d,p)
Mn1···B1	2.144(2)	2.141	2.122
Mn1−C101	1.801(2)	1.799	1.788
Mn1−C102	1.808(2)	1.789	1.780
Mn1−C103	1.805(2)	1.789	1.780
Mn1−N2	2.008(2)	2.021	2.007
Mn1−H200	1.66(2)	1.722	1.713
Mn1−H300	1.71(2)	1.722	1.713
B1−N1	1.501(3)	1.508	1.509
B1−H100	1.09(2)	1.198	1.195
B1−H200	1.21(2)	1.304	1.292
B1−H300	1.24(2)	1.304	1.292
H200–Mn1–H300	68.3(10)	73.9	73.9
Mn1–H200–B1	95.2(13)	89.0	88.7
Mn1–H300–B1	91.9(12)	89.0	88.7
H200–B1–H300	101.3(14)	115.1	105.7

Table 2. Experimental (XRD) and calculated (DFT) interatomic distances (Å) and angles (°) in *fac*-[RuH(κ^3*N,H,H*-mapyBH$_3$)(CO)(P*i*Pr$_3$)] (**2**).

Atoms	XRD	ZORA-PW91/QZ4P	B3P86/6-31G(d,p)/LanL2DZ
Ru1···B1	2.213(2)	2.225	2.219
Ru1−C101	1.834(2)	1.853	1.856
Ru1−N2	2.125(2)	2.154	2.144
Ru1−P1	2.3132(6)	2.321	2.327
Ru1–H200	1.83(3)	1.857	1.881
Ru1−H300	1.80(3)	1.842	1.820
Ru1−H400	1.60(3)	1.610	1.589
B1−N1	1.513(3)	1.527	1.525
B1−H100	1.12(2)	1.202	1.198
B1−H200	1.28(3)	1.305	1.293
B1−H300	1.28(3)	1.318	1.316
H200–Ru1–H300	69.6(12)	70.9	70.7
Ru1–H200–B1	89.2(15)	87.6	86.6
Ru1–H300–B1	90.4(15)	87.9	88.6
H200–B1–H300	108.3(18)	109.9	110.4

Natural bond orbital (NBO) analyses on complexes **1** and **2** revealed that the bonding in their MH_2B parts can be appropriately described as a combination of two 3-centre-2-electron M–H–B interactions (as a representative example, Fig. 4 shows the bonding orbitals responsible for these interactions in compound **1**). As found in other borane complexes,[3e,14,16] the Wiberg bond indices (Wbi's), which are indicative of bond order,[17] of the M–H200 and M–H300 atom pairs are very small (0.28 in **1** and 0.22 and 0.26, respectively, in **2**; Fig. 5), indicating weak interactions. As both 3-centre-2-electron M–H–B interactions contribute to the M–B Wbi of **1** and **2** and as their values (0.47 and 0.41, respectively) are smaller (but not negligible) than the summation of the corresponding M–H200 and M–H300 Wbi's, it can be inferred that the attachment of each B–H bond to the corresponding metal atom is between κ^1*H* (Shimoi-type) and κ^2*B,H* (agostic-type). In compound **1**, both B–H200 and B–H300 bonds interact equally with the Mn atom. However, in the case of compound **2**, the fact that the Ru–H200 Wbi (0.22) is smaller than the Ru–H300 Wbi (0.26) suggests that the interaction of the Ru atom with the B–H200 bond is more agostic than that with the B–H300 bond.

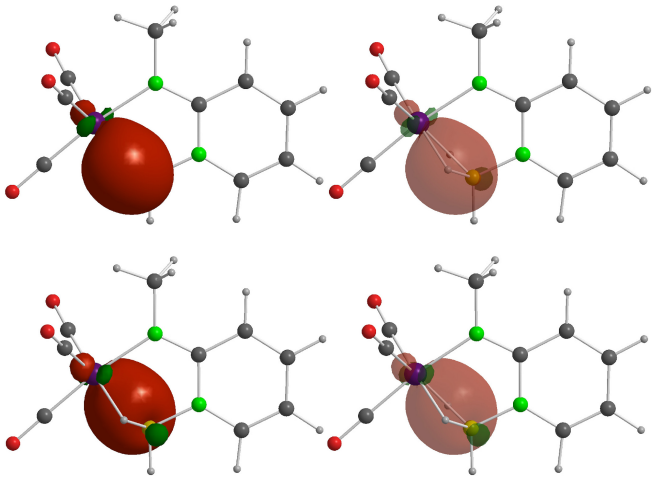

Fig. 4 Opaque (left) and transparent (right) views of the natural bond orbitals associated with the Mn1–H300–B1 (top; HOMO–12) and Mn1–H200–B1 (bottom; HOMO–13) 3-centre-2-electron interactions in complex **1** (isovalue: 0.05). Both orbitals have the same composition: 15.98% Mn, 37.99% B, 46.03 % H.

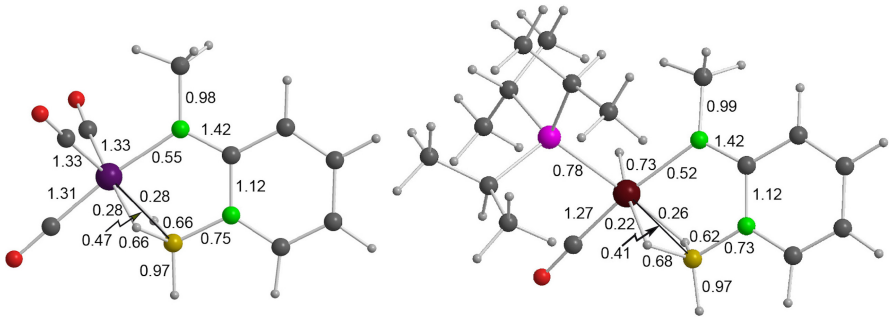

Fig. 5 Wiberg bond indices of selected interatomic interactions in compounds **1** (left) and **2** (right). Please, see Fig.s 2 and 3 for atom labeling.

The electron density associated with the bonding in compounds **1** and **2** was also theoretically investigated under the perspective of the QTAIM,[18] which has been recognized as a useful tool to study the bonding in transition metal complexes containing borane ligands.[3e,5d,8a–c,14,19] A selection of the obtained results is graphically represented in Fig. 6, which shows the bond paths (bp's), bond critical points (bcp's) and ring critical points (rcp's) associated with the bonds between the atoms contained in the MH_2B plane of the molecules. Table 3 contains the values of selected topological parameters of important interatomic interactions. Complementary QTAIM data are given in the ESI (Tables S2–S4 and Fig. S5 and S6).

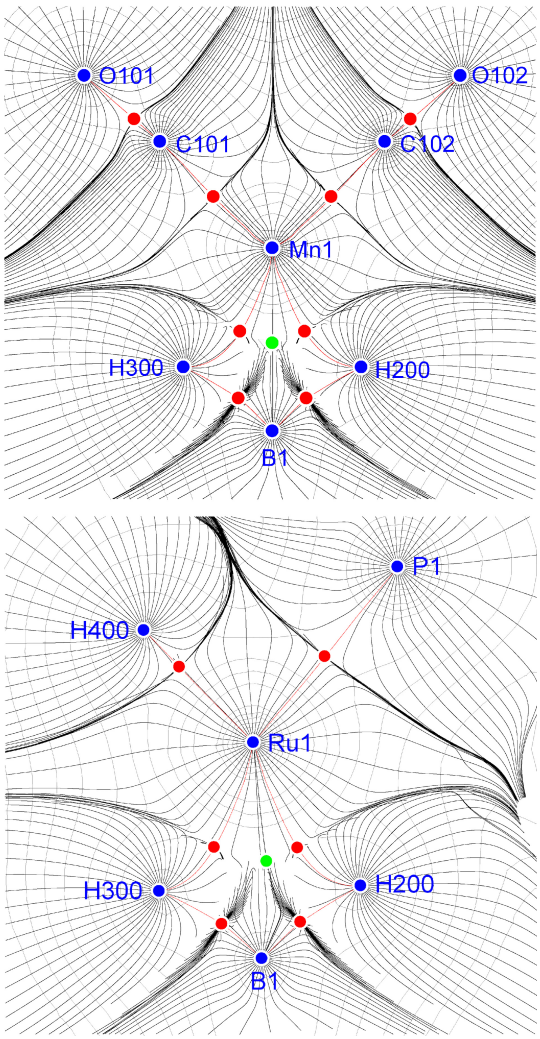

Fig. 6 Gradient trajectories mapped on total electron density plots (contour levels at 0.1 e $Å^{-3}$) in the MH_2B planes of compounds **1** (M = Mn; top) and **2** (M = Ru; bottom), showing the atomic basins, stationary points (blue circles), bp's (red lines), bcp's (red circles), and rcp's (green circles).

Table 3. Selected QTAIM topological parameters of selected interactions of complexes **1** and **2**

Comp.	Interaction	d^a (Å)	$\rho_b{}^b$ (e Å^{-3})	$\nabla^2\rho_b{}^c$ (e Å^{-5})	$\varepsilon_b{}^d$	δ(A–B)^e
1	Mn1···B1					0.160
	Mn1–H200	1.890	0.550	5.176	1.267	0.408
	Mn1–H300	1.880	0.551	5.275	1.245	0.411
	B1–H100	1.198	1.236	–9.271	0.008	0.557
	B1–H200	1.315	0.920	–3.743	0.252	0.389
	B1–H300	1.316	0.919	–3.728	0.253	0.388
2	Ru1···B1					0.191
	Ru1–H200	2.183	0.543	4.613	8.889	0.437
	Ru1–H300	2.040	0.557	4.962	2.518	0.466
	Ru1–H400	2.033	0.657	3.796	0.088	0.946
	B1–H100	1.202	1.217	–8.753	0.023	0.553
	B1–H200	1.315	0.929	–4.444	0.250	0.407
	B1–H300	1.329	0.898	–4.012	0.293	0.395

[a]Bond path length. [b]Electron density at the bcp. [c]Laplacian of the electron density at the bcp. [d]Ellipticity at the bcp. [e] Delocalization index.

Although Fig. 6 and Table 3 indicate that no bond path (and consequently no bcp) was found between the M and B atoms of **1** and **2**, a non-negligible δ(M–B) delocalization index was computed for each complex, 0.160 for **1** and 0.191 for **2**. As this integral parameter (not associated with a bcp) estimates the number of electron pairs that are delocalized between two atoms,[20] there should be a weak interaction between M and B that is not strong enough to be recognized as a bond by the QTAIM. This statement is also supported by the non-negligible M–B Wbi's shown in Fig. 4 and also by the experimental M–B distances, 2.1442(2) Å in **1** and 2.213(2) Å in **2**, which are slightly shorter than the summation of the average experimental (XRD) covalent radii of the corresponding atoms (0.84, 1.39 and 1.46 Å for B, Mn and Ru, respectively).[21] As a pure Shimoi-type coordination of a B–H bond should imply no M–B interaction, these data confirm the existence of some extent of agostic interaction in the attachment of the BH_2 group to the metal atom of **1** and **2**.

A quick view of Fig. 6 immediately allows the observation that the rcp associated with MH_2B ring of complex **1** is in a symmetric position while that of complex **2** is clearly displaced towards H200. Accordingly, the topological parameters given in Table 3 for the M–H200 and M–H300 interactions are equivalent in complex **1**, but some of them are notably different in complex **2**, in particular, the bond path length (d) and the ellipticity at the bcp (ε_b). In fact, the bond path of the Ru–H200 interaction is more curved and therefore longer (d = 2.183 Å) than that of the Ru–H300 interaction (d = 2.040 Å) and the ellipticity (ε_b) of the Ru–H200 interaction (8.889) is more than three

times greater than that of the Ru–H300 interaction (2.518). Therefore, while the M–H200 and M–H300 interactions are equivalent in complex **1**, they are different in complex **2**. As it has been previously shown that the Shimoi and the agostic attachments of a B–H bond to a metal atom have similar electron density at the M–H bcp (ρ_b) and similar Laplacian of the electron density at the M–H bcp ($\nabla^2\rho_b$), but different ellipticity at the bcp (ε_b), that of agostic-type being significantly greater than that of Shimoi-type,[14,22] the data given in Table 3 indicate that the type of interaction existing between the M atom of **1** and **2** and the borane B–H bonds is intermediate between those of Shimoi and agostic types and that, in complex **2**, the interaction of the B–H200 bond with the Ru atom is more agostic than that of the B–H300 bond.

Conclusions

The reactions of $[MnBr(MeCN)_2(CO)_3]$ or $[RuHCl(CO)(P\textit{i}Pr_3)_2]$ with $K[mapyBH_3]$ afford the octahedral complexes *fac*-$[Mn(\kappa^3\textit{N,H,H}\text{-}mapyBH_3)(CO)_3]$ (**1**) and *fac*-$[RuH(\kappa^3\textit{N,H,H}\text{-}mapyBH_3)(CO)(P\textit{i}Pr_3)]$ (**2**), in which the borane-containing ligand acts as a tripod $\kappa^3\textit{N,H,H}$-ligand through the amido N atom and through two H atoms of the BH_3 group.

Theoretical (DFT and QTAIM) gas-phase studies have shown that the attachment of the BH_3 group to the metal atom in **1** is symmetric and that it involves two B–H–M interactions that are intermediate between $\kappa^1\textit{H}$-BH (Shimoi-type) and $\kappa^2\textit{B,H}$-BH (agostic-type). Therefore, the slight asymmetry found in complex **1** in solid state by XRD has to be due to experimental errors, packing effects, or a combination of both, and that the 90° ideal coordination angle of octahedral complexes is adequate to symmetrically accommodate a BH_2 group in two adjacent coordination sites.

The symmetric structure found for the octahedral complex **1** in the gas phase also supports the proposal that the asymmetric coordination found for the BH_2 fragment in complex **2** (XRD, DFT, QTAIM) is not due to the octahedral coordination geometry of the complex but simply to the different *trans* influence of the hydride and phosphane ligands (that are *trans* to the H atoms of the BH_2 group). In complex **2**, the attachment of both borane B–H bonds to the metal atom is also intermediate between those of Shimoi and agostic types, but the B–H bond *trans* to the hydride interacts more agostically with the metal atom than the B–H bond that is *trans* to the phosphane.

These results complement a previous work in which we reported that the coordination of the BH_2 fragment of the $mapyBH_3$ ligand in the trigonal bipyramidal complexes $[M(\kappa^3\textit{N,H,H}\text{-}mapyBH_3)(cod)]$ (M = Rh, Ir) is asymmetric, not because it its influenced by the other ligands in the complex but because it occupies two equatorial

coordination sites whose ideal coordination angle (120°) is too wide to efficiently accommodate the BH_2 fragment in a symmetric manner.[14]

Experimental Section

General data. Solvents were dried over appropriate desiccating reagents and were distilled under argon before use. All reactions and manipulations were performed under argon using Schlenk-vacuum line techniques. The reaction products were vacuum-dried for several hours prior to being weighted and analyzed. The compounds $HmapyBH_3$,[14] $[MnBr(CO)_5]$[23] and $[RuHCl(CO)(P\textit{i}Pr_3)_2]$[24] were prepared following published procedures. All remaining reagents were purchased from commercial suppliers. The analytical instrumentation was as previously reported.[14]

***fac*-[Mn(κ^3*N,H,H*-mapyBH_3)$(CO)_3$] (1).** A toluene solution of $K[N(SiMe_3)_2]$ (1.2 mL, 0.5 M, 0.58 mmol) was added to a solution of $HmapyBH_3$ (58 mg, 0.48 mmol) in THF (15 mL). The resulting yellow solution was stirred at room temperature for 30 min and was added to a red acetonitrile solution of $[MnBr(MeCN)_2(CO)_3]$ (prepared *in situ* by stirring a solution of $[MnBr(CO)_5]$ (132 mg, 0.48 mmol) in 20 mL of acetonitrile at 50 °C for 80 min and subsequent concentration to *ca*. 5 mL). The resulting mixture was stirred at room temperature for 12 h. The solvent was removed under reduced pressure and the residue was extracted into hexane (3 x 5 mL). The filtered solution was evaporated to dryness to give **1** as an orange solid that was dried *in vacuo* (80 mg, 64 %). Anal. (%) Calcd for $C_9H_{10}BN_2MnO_3$ (M_W = 259.94 amu): C, 41.59; H, 3.88; N, 10.78; found: C, 41.62; H, 3.92; N, 10.75. (+)-ESI LRMS: *m/z* 261 $[M + H]^+$. IR (toluene): ν_{CO} 2040 (s), 1951 (vs, br) cm^{-1}. ^1H NMR (C_6D_6, 400.54 MHz, 298 K): δ 7.21 (d, $J_{H\text{-}H}$ = 6.8 Hz, 1 H, C*H*), 6.52 (t, $J_{H\text{-}H}$ = 6.8 Hz, 1 H, C*H*), 6.14 (d, $J_{H\text{-}H}$ = 6.8 Hz, 1 H, C*H*), 5.56 (t, $J_{H\text{-}H}$ = 6.8 Hz, 1 H, C*H*), 4.31 (q, br, $J_{H\text{-}11B}$ = 129 Hz, 1 H, *H*BH_2), 3.27 (s, 3 H, *Me*), –10.17 (q, br, $J_{H\text{-}11B}$ = 71 Hz, 2 H, Mn*H*$_2$B) ppm; the broad quartets at 4.31 and –10.17 ppm are transformed into two broad singlets in a $^1H\{^{11}B\}$ NMR spectrum. $^{13}C\{^1H\}$ NMR (C_6D_6, 100.62 MHz, 298 K): δ 222.4.1 (s, br, 2 *C*O), 219.1 (s, br, *C*O), 162.3 (*C*), 141.1 (*C*H), 134.4 (*C*H), 110.3 (*C*H), 105.0 (*C*H), 45.0 (*Me*) ppm. ^{11}B NMR (C_6D_6, 128.51 MHz, 298 K): δ 17.4 (dt, $J_{H\text{-}11B}$ = 129 and 71 Hz, *B*H_3) ppm; this signal collapses to a singlet in a $^{11}B\{^1H\}$ NMR spectrum.

***fac*-[RuH(κ^3*N,H,H*-mapyBH_3)(CO)(P*i*Pr_3)] (2).** A toluene solution of $K[N(SiMe_3)_2]$ (0.2 mL, 0.5 M, 0.10 mmol) was added to a solution of $HmapyBH_3$ (9.8 mg, 0.08 mmol) in toluene (7 mL). The resulting yellow suspension was stirred at room temperature for 30 min. Solid $[RuHCl(CO)(P\textit{i}Pr_3)_2]$ (39 mg, 0.08 mmol) was added and the mixture was stirred for 20 min. The resulting suspension was filtered and the filtrate was

concentrated to *ca.* 1 mL and was stored at –20 ^{o}C for 24 h to afford yellow crystals of compound **2**, which were isolated by decantation, washed with cold hexane (1 mL), and dried *in vacuo* (22 mg, 66 %). Anal. (%) Calcd for $C_{16}H_{32}BN_2OPRu$ (M_W = 411.29 amu): C, 46.72; H, 7.84; N, 6.81; found: C, 46.74; H, 7.87; N, 6.78. (+)-ESI LRMS: *m/z* 411 $[M - H]^+$. IR (toluene): ν_{CO} 1933 (s) cm^{-1}. ^{1}H NMR (C_6D_6, 400.54 MHz, 298 K): δ 7.57 (d, $J_{H\text{-}H}$ = 7.4 Hz, 1 H, C*H* of mapy), 6.61 (t, $J_{H\text{-}H}$ = 7.4 Hz, 1 H, C*H* of mapy), 6.36 (d, $J_{H\text{-}H}$ = 7.4 Hz, 1 H, C*H* of mapy), 5.63 (t, $J_{H\text{-}H}$ = 7.4 Hz, 1 H, C*H* of mapy), 4.45 (q, br, $J_{H\text{-}11B}$ = 113 Hz, 1 H, *H*BH_2), 3.70 (s, 3 H, *Me* of mapy), 2.00 (m, 3 H, 3 C*H* of P*i*Pr$_3$), 1.18 (m, 18 H, 6 Me of P*i*Pr$_3$), –4.35 (q, br, $J_{H\text{-}11B}$ = 65 Hz, 1 H, Ru*H*B), –6.52 (q, br, $J_{H\text{-}11B}$ = 65 Hz, 1 H, Ru*H*B), –11.68 (d, $J_{H\text{-}P}$ = 24.0 Hz, Ru*H*) ppm; the broad quartets at 4.45, –4.35, and –6.52 ppm are transformed into a triplet ($J_{H\text{-}H}$ = 8.0 Hz), a broad singlet and a doublet ($J_{H\text{-}H}$ = 8.0 Hz), respectively, in a ^{1}H{^{11}B} NMR spectrum. ^{13}C{^{1}H} NMR (C_6D_6, 100.62 MHz, 298 K): δ 162.3 (*C*), 142.9 (*C*H), 134.2 (*C*H), 109.6 (*C*H), 103.8 (*C*H), 47.3 (*Me*), 27.11 (d, $J_{C\text{-}P}$ = 22.9 Hz, *C*H of P*i*Pr$_3$), 20.1 (s, *Me* of P*i*Pr$_3$), 19.0 (s, *Me* of P*i*Pr$_3$) ppm. ^{11}B NMR (C_6D_6, 128.51 MHz, 298 K): δ 9.2 (dt, $J_{H\text{-}11B}$ = 113 and 65 Hz, *B*H_3) ppm; this signal collapses to a singlet in a ^{11}B{^{1}H} NMR spectrum. ^{31}P{^{1}H} NMR (C_6D_6, 128.51 MHz, 298 K): δ 80.3 (s) ppm.

X-ray crystallography. Crystals of **1** and **2** were analyzed by X-ray diffraction. A selection of crystal, measurement, and refinement data is given in the ESI (Table S1). Diffraction data were collected on an Oxford Diffraction Xcalibur Onyx Nova single crystal diffractometer. Empirical absorption corrections were applied using the SCALE3 ABSPACK algorithm as implemented in CrysAlisPro RED.[25] The structures were solved using SIR-97.[26] Isotropic and full matrix anisotropic least square refinements were carried out using SHELXL.[27] All non-H atoms were refined anisotropically. The hydrogen atoms of the BH_3 moieties of **1** and **2** and the hydride ligand of **2** were located in Fourier maps and were refined without constraints. The remaining hydrogen atoms were set in calculated positions and refined riding on their parent atoms. The WINGX program system[28] was used throughout the structure determinations. The molecular plots were made with MERCURY.[29] CCDC deposition numbers: 1524082 (**1**) and 1524083 (**2**).

Theoretical studies. DFT computations with non-relativistic wavefunctions were performed with the GAUSSIAN09 program package,[30] using the hybrid B3P86 hybrid functional[31] and the all-electron 6-31G(d,p) or 6-311++G(3df,3pd) basis sets for all atoms except Ru, the former for the geometry optimization processes and the latter for the single-point electronic structure calculations at the optimized geometries. The LanL2DZ effective core potential[32] and the large all-electron WTBS[33] basis sets were

used for the Ru atom, the former for the geometry optimization and the latter for the electronic structure calculation. The NBO[34] calculations were performed at the B3P86/6-31G(d,p) (**1**) and B3P86/6-31G(d,p)/LanL2DZ (**2**) levels of theory.

Computations with relativistic wavefunctions were performed using the scalar ZORA hamiltonian, the PW91 density functional and the all-electron relativistic QZ4P basis set for all atoms,[35] as implemented in the ADF2012 program package,[36] for the geometry optimizations, and the hybrid B1PW91 functional with relativistic QZ4P basis sets were for single-point electronic structure calculations at the optimized geometries.

The obtained non-relativistic and relativistic ground-state electronic wavefunctions, which were found to be stable, were then used for the QTAIM calculations, which included both local and integral properties and were carried out with the AIMAll,[37] AIM2000,[38] and DGrid[39] programs. The accuracy of the local properties was 1.0 x 10^{-10} (from the gradient of the electron density at the bcp's), whereas that of the integral properties was finally set at least at 1.0 x 10^{-4} (from the Laplacian of the integrated electron density). As expected for molecules containing a 3d transition metal (Mn), both the relativistic and non-relativistic calculations gave similar QTAIM results in the case of compound **1**; however, the use of relativistic calculations was essential in order to find all the expected bond and ring critical points of the Ru complex **2**.

Acknowledgments

This work has been supported by MINECO-FEDER projects (CTQ2013-40619-P, CTQ2016-75218-P, CTQ2014-51912-REDC, MAT2013-40950-R, and RYC2012-10491) and by research grants from the Government of Asturias (GRUPIN14-009 and GRUPIN14-060).

References

1 (a) H. C. Johnson, T. N. Hooper and A. S. Weller, *Top. Organomet. Chem*., 2015, **49**, 153; (b) E. M. Leitao, T. Jurca and I. Manners, *Nat. Chem*., 2013, **5**, 817; (c) T. J. Clark, K. Lee and I. Manners, *Chem. Eur. J.,* 2006, **12**, 8634.

2 (a) A. Rossin and M. Peruzzini, *Chem. Rev.,* 2016, **116**, 8848; (b) H. C. Johnson, T. N. Hooper and A. S. Weller, in *Synthesis and Application of Organoboron Compounds*; vol. 49; E. Fernández and A. Whiting, Eds.; Springer International Publishing, New York City, NY, 2015, pp. 153–220.

3 (a) M. A. Esteruelas, P. Nolis, M. Oliván, E. Oñate, A. Vallribera and A. Vélez, *Inorg. Chem.,* 2016, **55**, 7176; (b) M. Roselló-Merino, R. J. Rama, J. Díez and S. Conejero, *Chem. Comm.,* 2016, **52**, 8389; (c) X. Zhang, L. Kam and T. J. Williams,

Dalton Trans., 2016, **45**, 7672; (d) A. M. Lunsford, J. H. Blank, S. Moncho, S. C. Haas, S. Muhammad, E. N. Brohers, M. Y. Darensbourg and A. A. Bengali, *Inorg. Chem.,* 2016*,* **55**, 964; (e) A. E. Nako, A. J. P. White and M. R. Crimmin, *Dalton Trans.,* 2015, **44**, 12530; (f) D. F. Schreiber, C. O'Connor, C. Grave, Y. Ortin, H. Müller-Bunz and A. D. Phillips, *ACS Catal.,* 2012, **2**, 2505; (g) T. Miyazaki, Y. Tanabe, M. Yuki, Y. Miyake and Y. Nishibayashi, *Organometallics,* 2011, **30**, 2394; (h) R. Dallanegra, A. B. Chaplin and A. S. Weller, *Angew. Chem. Int. Ed.,* 2009, **48**, 6875.

4 (a) C. J. Wallis, G. Alcaraz, A. S. Petit, A. I. Poblador-Bahamonde, E. Clot, C. Bijani, L. Vendier and S. Sabo-Etienne, *Chem. Eur. J.,* 2015, **21**, 13080; (b) J. R. Vance, A. Schäfer, A. P. M. Robertson, K. Lee, J. Turner, G. R. Whittell and I. Manners, *J. Am. Chem. Soc.,* 2014, **136**, 3048; (c) H. C. Johnson, E. M. Leitao, G. R. Whittell, I. Manners, G. C. Lloyd-Jones and A. S. Weller, *J. Am. Chem. Soc.,* 2014, **136**, 9078; (d) A. N. Marziale, A. Friedrich, I. Klopsch, M. Drees, V. R. Celinski, J. Schmedt auf der Günne and S. Schneider, *J. Am. Chem. Soc.,* 2013, **135**, 13342; (e) L. J. Sewell, G. C. Lloyd-Jones and A. S. Weller, *J. Am. Chem. Soc.,* 2012, **134**, 3598; (f) C. J. Stevens, R. Dallanegra, A. B. Chaplin, A. S. Weller, S. A. Macgregor, B. Ward, D. McKay, G. Alcaraz and S. Sabo-Etienne, *Chem. Eur. J.,* 2011*,* **17**, 3011; (g) A. B. Chaplin and A. S. Weller, *Inorg. Chem.,* 2010, **49**, 1111.

5 (a) M. W. Drover, E. G. Bowes, L. L. Schafer, J. A. Love and A. S. Weller, *Chem. Eur. J.,* 2016, **20**, 6793; (b) D. Vidovoc, D. A. Addy, T. Krämer, J. McGrady and S. Aldridge, *J. Am. Chem. Soc.,* 2011, **133**, 8494; (c) H. C. Johnson, A. P. M. Robertson, A. B. Chaplin, L. J. Sewell, A. L. Thompson, M. F. Haddow, I. Manners and A. S. Weller, *J. Am. Chem. Soc.,* 2011, **133**, 11076; (d) D. J. Wolstenholme, K. T. Traboulsee, A. Decken and G. S. McGrady, *Organometallics,* 2010, **29**, 5769; (e) G. Alcaraz, A. B. Chaplin, C. J. Stevens, E. Clot, L. Vendier, A. S. Weller and S. Sabo-Etienne, *Organometallics,* 2010, **29**, 5591. (f) M. C. Macinnis, R. McDonald, M. J. Ferguson, S. Tobisch and L. Turculet, *J. Am. Chem. Soc.*, 2011, **133**, 13622. (g) G. Alvaraz, L. Vendier, E. Clot and S. Sabo-Etienne, *Angew. Chem. Int. Ed.,* 2010, **49**, 918. (h) C. Y. Tang, A. L. Thompson and S. Aldridge, *Angew. Chem. Int. Ed.,* 2010, **49**, 921.

6 (a) K. A. Erickson, J. P. W. Stelmach, N. T. Mucha and R. Waterman, *Organometallics*, 2015, **34**, 4693; (b) H. Dong and H. Berke, *J. Organomet. Chem.,* 2011, **696**, 1803; (c) Y. Jiang, O. Blacque, T. Fox, C. M. Frech and H. Berke, *Organometallics,* 2009, **28**, 5493.

7 (a) G. Alcaraz and S. Sabo-Etienne, *Angew. Chem. Int. Ed.,* 2010, **49**, 7170; (b) M. Shimoi, S. I. Nagai, M. Ichikawa, Y. Kawano, K. Katoh, M. Uruichi and H. Ogino, *J. Am. Chem. Soc.,* 1999, **121**, 11704; (c) G. J. Kubas, *Metal Dihydrogen and σ-Bond Complexes*; Springer: New York City, NY, 2001.

8 (a) K. Bakthavachalam, K. Yuvaraj, M. Zafar and S. Ghosh, *Chem. Eur. J.,* 2016, **22**, 17291; (b) K. Saha, B. Joseph, R. Ramalakshmi, R. S. Anju, B, Varghese and S. Ghosh, *Chem. Eur. J.,* 2016, **22**, 7871; (c) R. Ramalakshmi, K. Saha, D. K. Roy, B. Varghese, A. K. Phukan and S. Gosh, *Chem. Eur. J.,* 2015, **21**, 17191; (d) D. K. Roy, R. Borthakur, S. Bhattacharyya, V. Ramkumar and S. Ghosh, *J. Organomet. Chem.,* 2015, **799**–**800**, 132.

9 Y. Huang and D. W. Stephan, *Organometallics,* 1995, **14**, 2835.

10 (a) T. F. van Dijkman, H, M. de Brujin, M. A. Siegler and E. Bouwman, *Eur. J. Inorg. Chem.,* 2015, 5387; (b) H. V. R. Dias and H. L. Lu, *Inorg. Chem.,* 2000, **39**, 2246; (c) H. V. R. Dias, H. L. Lu, J. D. Gorden and W. Jin, *Inorg. Chem.,* 1996, **35**, 3935.

11 (a) D. H. Nguyen, H. Lauréano, S. Jugé, P. Kalck, J.-C. Daran, Y. Coppel, M. Urrutigoiti and M. Gouygou, *Organometallics,* 2009, **28**, 6288; (b) N. Merle, C. G. Frost, G. Kociok-Köhn, M. C. Willis and A. S. Weller, *Eur. J. Inorg. Chem.,* 2006, 4068; (c) N. Merle, G. Kociok-Köhn, M. F. Mahon, C. G. Frost, G. D. Ruggiero, A. S. Weller and M. C. Willis, *Dalton Trans.,* 2004, 3883; (d) O. Volkov, R. Macías, N. P. Rath and L. Barton, *Inorg. Chem.,* 2002, **41**, 5837; (e) M. Ingleson, N. J. Patmore, G. D. Ruggiero, C. G. Frost, M. F. Mahon, M. C. Willis and A. S. Weller, *Organometallics,* 2001, **20**, 4434.

12 (a) M. W. Drover, E. G. Bowes, L. L. Schafer, J. A. Love and A. S. Weller, *Chem. Eur. J.,* 2016*,* **22**, 6793; (b) M. W. Drover, L. L. Schafer and J. A. Love, *Angew. Chem. Int. Ed.,* 2016, **55**, 3181; (c) M. W. Drover, H. C. Johnson, L. L. Schafer, J. A. Love and A. S. Weller, *Organometallics,* 2015, **34**, 3849; (d) G. Ganguly, T. Malakar and A. Paul, *ACS Catal.,* 2015, **5**, 2754; (e) T.-P. Lin and J. C. Peters, *J. Am. Chem. Soc.,* 2014, **136**, 13672; (f) A. Cassen, Y. Gloaguen, L. Vendier, C. Duhayon, A. Poblador-Bahamonde, C. Raynaud, E. Clot, G. Alcaraz and S. Sabo-Etienne, *Angew. Chem. Int. Ed.,* 2014, **53**, 7569; (g) T. Stahl, K. Müther, Y. Ohki, K. Tatsumi and M. Oestreich, *J. Am. Chem. Soc.,* 2013, **135**, 10978; (h) Y. Gloaguen, G. Alcaraz, A. S. Petit, E. Clot, Y. Coppel, L. Vendier and S. Sabo-Etienne, *J. Am. Chem. Soc.,* 2011, **133**, 17232; (i) M. A. Rankin, K. D. Hesp, G. Schatte, R. McDonald and M. Stradiotto, *Dalton Trans*., 2009, 4756; (j) Y.

Gloaguen, G. Alcaraz, A.-F. Pecharman, E. Clot, L. Vendier and S. Sabo-Etienne, *Angew. Chem. Int. Ed.,* 2009, **48**, 2964; (k) J. S. Figueroa, J. G. Melnick and G. Parkin, *Inorg. Chem.,* 2006, **45**, 7056; (l) N. Merle, C. G. Frost, G. Kociok-Köhn, M. C. Willis and A. S. Weller, *J. Organomet. Chem.,* 2005, **690**, 2829.

13 M. W. Drover, E. G. Bowes, J. A. Love and L. L. Schafer, *Organometallics,* 2017, **36**, 331.

14 J. Brugos, J. A. Cabeza, P. García-Álvarez, A. R. Kennedy, E. Pérez-Carreño and J. F. Van der Maelen, *Inorg. Chem.,* 2016, **55**, 8905.

15 (a) K. M. Anderson and A. G. Orpen, *Chem. Commun.,* 2001, 2682; (b*)* R. H. Crabtree, *The Organometallic Chemistry of the Transition Metals* (4th ed.), Wiley-Interscience, New Jersey, 2005.

16 M. L. Buil, J. J. F. Cardo, M. A. Esteruelas, I. Fernández and E. Oñate, *Organometallics,* 2015, **34**, 547.

17 K. B. Wiberg, *Tetrahedron,* 1968, **24**, 1083.

18 (a) R. F. W. Bader, *Atoms in Molecules, a Quantum Theory*; Clarendon Press, Oxford, UK, 1990; (b) P. L. A. Popelier, *Atoms in Molecules, an Introduction*; Prentice Hall, Harlow, UK, 2000; (c) *The Quantum Theory of Atoms in Molecules*; Matta, C. F.; Boyd, R. J., Eds.; Wiley-VCH, Weinheim, Germany, 2007.

19 (a) D. Sharmila, B. Mondal, R. Ramalashmi, S. Kundu, B. Varghese and S. Gosh, *Chem. Eur. J.,* 2015, **23**, 5074; (b) K. D. Hesp, F. O. Kannemann, M. A. Rankin, R. McDonald, M. J. Ferguson and M. Stradiotto, *Inorg. Chem.,* 2011, **50,** 2431; (c) G. Bénac-Lestrille, U. Helmstedt, L. Vendier, G. Alcaraz, E. Clot and S. Sabo-Etienne, *Inorg. Chem.,* 2011, **50**, 11039.

20 See, for example: (a) C. Gatti, *Z. Kristallogr.,* 2005, **220**, 339; (b) P. Macchi and A. Sironi, *Coord. Chem. Rev.,* 2003, **238**, 383; (c) L. J. Farrugia, C. Evans, H. M. Senn, M. M. Aänninen and R. Sillanpää, *Organometallics,* 2012, **31**, 2559; (d) J. F. Van der Maelen and J. A. Cabeza, *Theor. Chem. Acc.,* 2016, **135**, 64; (e) J. F. Van der Maelen and J. A. Cabeza, *Inorg. Chem.,* 2012, **51**, 7384; (f) J. F. Van der Maelen, S. García-Granda and J. A. Cabeza, *Comput. Theor. Chem.,* 2011, **968**, 55; (g) J. A. Cabeza, J. F. Van der Maelen and S. García-Granda, *Organometallics,* 2009, **28**, 3666.

21 B. Cordero, V. Gómez, A. E. Platero-Prats, M. Revés, J. Echeverría, E. Cremades, F. Barragán and S. Álvarez, *Dalton Trans.,* 2008, 3832.

22 A. Kumar, N. A. Beattie, S. D. Pike, S. A. MacGregor and A. S. Weller, *Angew. Chem. Int. Ed.,* 2016, **55**, 6651.

23 K. J. Reimer and A. L. Shaver, *Inorg. Synth.*, 1990, **28**, 154.

24 M. A. Esteruelas and H. Werner, *J. Organomet. Chem.*, 1986, **303**, 221.

25 *CrysAlisPro RED*, version 1.171.37.35, Oxford Diffraction Ltd., Oxford, UK, 2014.

26 A. Altomare, M. C. Burla, M. Camalli, G. L. Cascarano, C. Giacovazzo, A. Guagliardi, A. G. C. Moliterni, G. Polidori and R. Spagna, *J. Appl. Crystallogr.,* 1999, **32**, 115.

27 *SHELXL-2014*: G. M. Sheldrick, *Acta Cryst.,* 2008, **A64**, 112.

28 *WINGX*, version 2013.3: L. J. Farrugia, *J. Appl. Crystallogr.,* 1999, **32**, 837.

29 *MERCURY*, CSD 3.8 (build RC2), Cambridge Crystallographic Data Centre, Cambridge, UK, 2016.

30 M. J. Frisch, G. W. Trucks, H. B. Schlegel, G. E. Scuseria, M. A. Robb, J. R. Cheeseman, G. Scalmani, V. Barone, G. A. Petersson, H. Nakatsuji, X. Li, M. Caricato, A. Marenich, J. Bloino, B. G. Janesko, R. Gomperts, B. Mennucci, H. P. Hratchian, J. V. Ortiz, A. F. Izmaylov, J. L. Sonnenberg, D. Williams-Young, F. Ding, F. Lipparini, F. Egidi, J. Goings, B. Peng, A. Petrone, T. Henderson, D. Ranasinghe, V. G. Zakrzewski, J. Gao, N. Rega, G. Zheng, W. Liang, M. Hada, M. Ehara, K. Toyota, R. Fukuda, J. Hasegawa, M. Ishida, T. Nakajima, Y. Honda, O. Kitao, H. Nakai, T. Vreven, K. Throssell, J. A. Montgomery, Jr., J. E. Peralta, F. Ogliaro, M. Bearpark, J. J. Heyd, E. Brothers, K. N. Kudin, V. N. Staroverov, T. Keith, R. Kobayashi, J. Normand, K. Raghavachari, A. Rendell, J. C. Burant, S. S. Iyengar, J. Tomasi, M. Cossi, J. M. Millam, M. Klene, C. Adamo, R. Cammi, J. W. Ochterski, R. L. Martin, K. Morokuma, O. Farkas, J. B. Foresman and D. J. Fox, *GAUSSIAN09*, revision A.02, Gaussian, Inc., Wallingford, CT, 2016

31 (a) C. Lee, W, Yang and R. G. Parr, *Phys. Rev. B* 1988, **37**, 785; (b) J. P. Perdew, *Phys. Rev. B* 1986, **33**, 8822; (c) A. D. Becke, *J. Chem. Phys.,* 1993, **98**, 5648.

32 P. J. Hay and W. R. Wadt, *J. Chem. Phys.,* 1985, **82**, 299.

33 (a) S. Huzinaga and B. Miguel, *Chem. Phys. Lett.,* 1990, **175**, 289; (b) S. Huzinaga and M. Klobukowski, *Chem. Phys. Lett.,* 1993, **212**, 260.

34 E. Glendening, J. K. Badenhoop, A. E. Reed, J. E. Carpenter, J. A. Bohmann, C. M. Morales, C. R. Landis and F. Weinhold, *Natural Bond Orbital*, version 6.0; Theoretical Chemistry Institute, University of Wisconsin, Madison, 2013.

35 E. van Lenthe and E. J. Baerends, *J. Comput. Chem*., 2003, **24**, 1142.

36 E. J. Baerends, T. Ziegler, J. Autschbach, D. Bashford, A. Bérces, F. M. Bickelhaupt, C. Bo, P. M. Boerrigter, L. Cavallo, D. P. Chong, L. Deng, R. M. Dickson, D. E. Ellis, M. van Faassen, L. Fan, T. H. Fischer, C. Fonseca-Guerra, M. Franchini, A. Ghysels, A. Giammona, S. J. A. van Gisbergen, A. W. Götz, J. A. Groeneveld, O. V. Gritsenko, M. Grüning, S. Gusarov, F. E. Harris, P. van den Hoek, C. R. Jacob, H. Jacobsen, L. Jensen, J. W. Kaminski, G. van Kessel, F. Kootstra, A. Kovalenko, M. V. Krykunov, E. van Lenthe, D. A. McCormack, A. Michalak, M. Mitoraj, S. M. Morton, J. Neugebauer, V. P. Nicu, L. Noodleman, V. P. Osinga, S. Patchkovskii, M. Pavanello, P. H. T. Philipsen, D. Post, C. C. Pye, W. Ravenek, J. I. Rodríguez, P. Ros, P. R. T. Schipper, G. Schreckenbach, J. S. Seldenthuis, M. Seth, J. G. Snijders, M. Solà, M. Swart, D. Swerhone, G. te Velde, P. Vernooijs, L. Versluis, L. Visscher, O. Visser, F. Wang, T. A. Wesolowski, E. M. van Wezenbeek, G. Wiesenekker, S. K. Wolff, T. K. Woo and A. L. Yakovlev, *AFD2012*, Theoretical Chemistry, Vrije Universiteit, Amsterdam, The Netherlands, 2012.

37 T. A. Keith, *AIMAll*, version 15.09.27, T. K. Gristmill Software, Overland Park, Kansas, 2015.

38 F. Biegler-König and J. Schönbohm, *J. Comput. Chem.,* 2002, **23**, 1489.

39 M. Kohout, *DGrid 4.6*, Max Planck Institute for Physical Chemistry of Solids, Dresden, Germany, 2011.

Figure and text for the Table of Contents

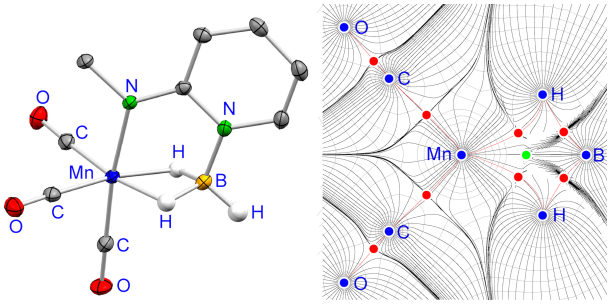

The borane adduct of the 2-(methylamido)pyridine anion has been incorporated to octahedral metal (Mn, Ru) complexes and their bonding has been studied by theoretical methods (DFT, QTAIM).